

# QARV: Quantization-Aware ResNet VAE for Lossy Image Compression

Zhihao Duan, Ming Lu, Jack Ma, Zhan Ma, and Fengqing Zhu

**Abstract**—We consider the problem of lossy image compression, a fundamental problem in both information theory and many real-world applications. We begin by reviewing the relationship between variational autoencoders (VAEs), a powerful class of deep generative models, and rate-distortion theory, the theoretical foundation for lossy compression. By combining the ResNet VAE architecture and techniques including test-time quantization and quantization-aware training, we present a quantization-aware ResNet VAE (QARV) framework for lossy image compression. For sake of practical usage, we propose a new neural network architecture for fast decoding, and we introduce an adaptive normalization operation for variable-rate coding. QARV employs a hierarchical progressive coding structure, supports continuously variable-rate compression with fast entropy coding, and gives a better rate-distortion efficiency than existing baseline methods. Code is made publicly available at <https://github.com/duanzhihao/lossy-vae>.

**Index Terms**—Lossy image compression, variational autoencoder, deep learning.

## 1 INTRODUCTION

EFFICIENT data storage/communication and generative modeling of data distribution are fundamentally connected through the principle of information compression. As for discrete data, seeking a better lossless compression algorithm is equivalent to the maximum-likelihood learning of a generative model. Indeed, many modern image generative models are also the best-performing lossless image coding methods [1], [2].

For continuously-valued data, however, only lossy compression is feasible. The theoretical limit for lossy compression is described by the rate-distortion (R-D) theory [3]. Interestingly, a specific type of generative model, Variational Autoencoders (VAEs), has been shown to be deeply connected to the R-D theory. VAEs are a latent variable model where both the posterior (of the latent variable given data) and the prior (of the latent variable without observation of data) are parameterized by learnable neural networks. With a distortion metric specified, it is shown that VAEs learn to compress data by minimizing an upper bound on the information R-D function of the data [4], where the bound is tight if the neural networks are sufficiently expressive.

Modern VAEs typically employ a hierarchical architecture called ResNet VAE [5]. ResNet VAEs have been used for various tasks such as image distribution modeling [6], lossless compression [7], and estimating the R-D function for images [4], achieving prominent performance in all of them. Motivated by the promising performance of ResNet VAEs and their theoretical connection to lossy compression, various research has been done for adapting them to practical lossy image compression. This is not as straightforward as it may look, because ResNet VAEs employ continuously-

valued latent variables, which are infeasible to be coded into bits using existing entropy coding algorithms (which require a discrete alphabet). One solution is to communicate stochastic samples using Relative Entropy Coding (REC) [8] algorithms. REC methods, however, either require a running time exponential to rate and are thus intractable [8] or suffer a codelength overhead [9]. Another line of research studies post-training quantization [10], but the resulting R-D performance is sub-optimal compared to existing transform coding-based methods.

Unlike the aforementioned works, we extend ResNet VAEs to practical lossy image compression through a combination of test-time quantization-aware training. At test time, we quantize the latent variables by elementwise uniform quantization, which is arguably one of the simplest quantization methods. To make training quantization-aware, we simulate uniform quantization by additive uniform noise, a standard choice in learned compression methods [11]. The use of additive uniform noise is equivalent to setting all posteriors in the ResNet VAE to be a (conditional) uniform distribution. We parameterize the priors using a Gaussian convolved with a uniform distribution, following the successful Hyperprior model [12]. Under this configuration, we are able to turn ResNet VAEs into practical lossy image codecs while keeping all its advantages, *i.e.*, hierarchical progressive coding and efficient computation, as demonstrated in our recent work [13]. Our model can be viewed as a generalization of several context entropy models proposed by recent works, including spatially AR models [14], [15] and the channelwise AR model [16], which we show in Sec. 3.3.

In this paper, we further expand our previous work in two ways to step toward a real-world application of learning-based image codecs. In many real-world applications of image compression, *e.g.*, image sharing on social media, images are encoded only once but are decoded far more times, in which case the decoding complexity is more critical than for encoding. ResNet VAEs naturally have a bias to-

- Z. Duan, J. Ma, and F. Zhu are with the Elmore Family School of Electrical and Computer Engineering, Purdue University, West Lafayette, Indiana 47907, U.S.A.  
E-mail: [duan90@purdue.edu](mailto:duan90@purdue.edu), [ma699@purdue.edu](mailto:ma699@purdue.edu), [zhu0@purdue.edu](mailto:zhu0@purdue.edu).
- M. Lu and Z. Ma are with the School of Electronic Science and Engineering, Nanjing University, Nanjing, Jiangsu 210093, China.  
E-mail: [luming@smail.nju.edu.cn](mailto:luming@smail.nju.edu.cn), [mazhan@nju.edu.cn](mailto:mazhan@nju.edu.cn).

ward fast decoding (although slower encoding) due to their bi-directional inference structure, and we further exploit this fact by shifting computation from decoding to encoding. We also introduce a new variable-rate compression method, namely adaptive layer normalization (AdaLN), that can be readily used in modern neural network blocks in a plug-and-play fashion. Combining these techniques, we present a new model, QARV (for quantization-aware ResNet VAE), that compresses images with continuously adjustable rates using a single model. Experimental results confirm that QARV outperforms existing published lossy image codecs in terms of both BD-rate and decoding speed on CPUs and GPUs.

Our contributions are summarized as follows, where the first contribution is an extended analysis of our previous work [13], and the rest are new in this paper.

- We give an extended theoretical explanation of the quantization-aware ResNet VAE (QARV) framework;
- We present a new block architecture for QARV that enables faster decoding and better R-D performance;
- We provide a new method, adaptive layer normalization (AdaLN), for variable-rate compression;
- Overall, we propose a new neural network model and conduct extensive experiments around it. Experimental results demonstrate that our model achieves better compression efficiency than existing open-source methods in terms of both decoding speed and R-D performance.

## 2 RELATED WORKS: FROM TRANSFORM CODING TO CODING WITH GENERATIVE MODELS

Starting with the traditional transform coding-based methods, we systematically review existing methods for lossy image compression. We then review the connection between VAEs and lossy compression, which largely motivates the design of our approach.

### 2.1 Lossy Image Compression by Transform Coding

In conventional image codecs such as JPEG [17], JPEG 2000 [18], and VVC intra [19], an orthogonal linear transformation such as discrete cosine transform (DCT) and discrete wavelet transform (DWT) is applied to convert image pixels into transform coefficients. A probabilistic model is built for the transform coefficients, which are subsequently quantized and coded into bits using entropy coding algorithms.

Most learning-based image compression methods follow the same transform coding paradigm but in a non-linear way [20]. These methods use a pair of encoder and decoder, both parameterized by deep neural networks (DNNs), in place of the linear orthogonal transforms. To enable rate-distortion optimization, an *entropy model* (also parameterized by DNNs) is built for the compressed representation to estimate the number of bits needed for coding in a differentiable way. To improve compression efficiency, existing works have explored efficient neural network blocks, such as residual networks [21], self-attention [22], and transformers [23], [24], [25], as well as develop more expressive entropy models, such as hierarchical [12], [26] and autoregressive models [14], [15], [16], [27].

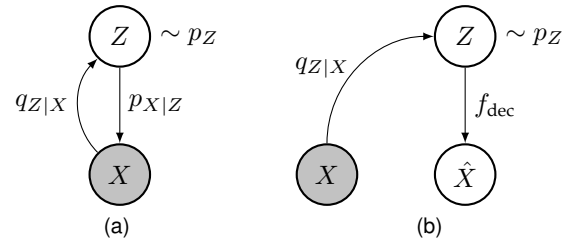


Fig. 1. Probabilistic model of (a) a one-layer VAE in its original form and (b) a one-layer VAE for lossy compression, where  $X$  is data,  $Z$  is the latent variable, and  $\hat{X}$  is the reconstruction.

### 2.2 Variational Autoencoder and its Connection to the Rate-Distortion Theory

Variational autoencoder (VAE) [28] is a class of latent variable models where conditional probability distributions are parameterized by neural networks. Let  $X$  be the random variable representing data (in our case, images) with an unknown data distribution  $p_{\text{data}}$ . In its original form [28], VAE models data by a joint distribution

$$p_{X,Z}(x, z) = p_{X|Z}(x|z) \cdot p_Z(z), \quad (1)$$

where  $Z$  is the assumed *latent variable*,  $p_Z$  is the *prior distribution* for  $Z$ , and  $p_{X|Z}$  is the conditional data likelihood of  $X$  given  $Z$  (often referred to as the decoder). Both  $p_Z$  and  $p_{X|Z}$  are parameterized by neural networks. To perform variational inference of  $Z$  given  $X$ , VAE also defines an *approximate posterior*  $q_{Z|X}$  (also known as the encoder), which is again parameterized by neural networks. The probabilistic graphical model of VAE is shown in Fig. 1a.

The goal of VAE is to find the set of model parameters such that the marginal distribution  $p_X$  is close to the true data distribution  $p_{\text{data}}$ . This is done by minimizing a variational upper bound on the negative log-likelihood (NLL):

$$\begin{aligned} \mathcal{L} &\triangleq \mathbb{E}_{X \sim p_{\text{data}}, Z \sim q_{Z|X}} \left[ D_{\text{KL}}(q_{Z|X} || p_Z) + \log \frac{1}{p_{X|Z}(X|Z)} \right] \\ &\geq \mathbb{E}_{X \sim p_{\text{data}}} [-\log p_X(X)], \end{aligned} \quad (2)$$

where  $D_{\text{KL}}$  denotes the Kullback–Leibler (KL) divergence. By convention, the natural logarithm is used, so both NLL and  $\mathcal{L}$  have a unit of nats. When  $X$  is discrete, NLL is the lossless compression rate under the model  $p_X$ , and by minimizing  $\mathcal{L}$ , VAEs learn to losslessly compress data using as few bits as possible (more details in Sec. 2.4).

When  $X$  is continuous, in which case lossless compression is impossible, a different parameterization of VAE is used for lossy compression (shown in Fig. 1b). Instead of the data likelihood  $p_{X|Z}$ , a reconstruction  $\hat{X} = f_{\text{dec}}(Z)$  is introduced, where  $f_{\text{dec}}$  is a function representing the *decoder*. In practice,  $f_{\text{dec}}$  is typically implemented by a neural network that maps low-dimensional representations to the high-dimensional data space. Under this formulation, the loss function of VAE becomes

$$\mathcal{L} = \mathbb{E}_{X \sim p_{\text{data}}, Z \sim q_{Z|X}} \left[ D_{\text{KL}}(q_{Z|X} || p_Z) + \lambda \cdot d(X, \hat{X}) \right], \quad (3)$$

where  $\lambda$  is a scalar hyperparameter to trade-off the KL term (we will soon see it corresponds to rate) and distortion, and

$d$  is an arbitrary distortion measure, *e.g.*, the mean squared error (MSE). It can be shown that

$$\mathbb{E}_{X \sim p_{\text{data}}, Z \sim q_{Z|X}} [D_{\text{KL}}(q_{Z|X} \| p_Z)] \geq I(X, \hat{X}), \quad (4)$$

where the bound is tight if the neural network is powerful enough [4]. Combining Eq. 3 and Eq. 4, we can see that the VAE loss function is an upper bound on a Lagrangian relaxation of the information R-D function. For any  $\lambda > 0$ , minimizing Eq. 3 results in an R-D pair that is a (tight) upper bound on the true information R-D function.

### 2.3 Hierarchical VAEs

To model high-dimensional data such as images, hierarchical VAEs [5], [6], [29], [30] are proposed to improve the flexibility and expressiveness of VAEs. A hierarchical VAE employs a group of latent variables, denoted by  $Z_{1:N} \triangleq \{Z_1, Z_2, \dots, Z_N\}$ , where  $N$  is the total number of variables. An autoregressive model among them is assumed:

$$p_{Z_{1:N}}(z_{1:N}) = p_{Z_N|Z_{<N}}(z_N|z_{<N}) \cdots p_{Z_2|Z_1}(z_2|z_1) p_{Z_1}(z_1), \quad (5)$$

where  $Z_{<N}$  denotes  $\{Z_1, Z_2, \dots, Z_{N-1}\}$ . Typically,  $Z_1$  is low-dimensional and  $Z_N$  is high-dimensional. The low-to-high dimensional latent variables not only improve the flexibility of VAEs but also capture the coarse-to-fine nature of images.

A family of hierarchical VAEs, named ResNet VAE [5], provides the most promising performance in terms of NLL on images [6], [31]. Fig. 2b shows the encoding and decoding processes of a ResNet VAE for lossy compression. As a comparison, we also show the Hyperprior model [12] in Fig. 2a. ResNet VAEs are fundamentally different from Hyperprior VAEs in several important aspects:

- Both the encoding and decoding use the same top-down ordering of latent variables (while in Hyperprior VAE the two orderings are reversed);
- The latent variable  $Z_i$  is dependent on all  $Z_{<i}$ , for  $i \in \{1, 2, \dots, N\}$  (while in Hyperprior VAE the dependency is first-order Markov);
- The encoding is bi-directional, *i.e.*,  $Z_i$  is dependent on both  $X$  and  $Z_{<i}$  (while in Hyperprior VAE the encoding is bottom-up).

The loss function for training ResNet VAEs is the same as Eq. 3 but extended for multiple latent variables. For notational simplicity, we denote the posterior and prior for the  $i$ -th latent variable as  $q_i$  and  $p_i$ , respectively:

$$\begin{aligned} q_i(\cdot) &\triangleq q_{Z_i|X, Z_{<i}}(\cdot) \\ p_i(\cdot) &\triangleq p_{Z_i|Z_{<i}}(\cdot), \end{aligned} \quad (6)$$

where  $Z_{<1}$  is defined to be an empty set. Then, using this notation, the ResNet VAE loss function becomes

$$\mathcal{L} = \mathbb{E}_{X \sim p_{\text{data}}, Z_{1:N} \sim q_{Z_{1:N}|X}} \left[ \sum_{i=1}^N D_{\text{KL}}(q_i \| p_i) + d(X, \hat{X}) \right]. \quad (7)$$

### 2.4 Practical Coding with VAEs

For discrete data  $X$ , VAEs can be readily applied to perform lossless compression by using the bits-back coding algorithm [32]. Example methods for images include lossless image compression using a single-layer VAE [7] and

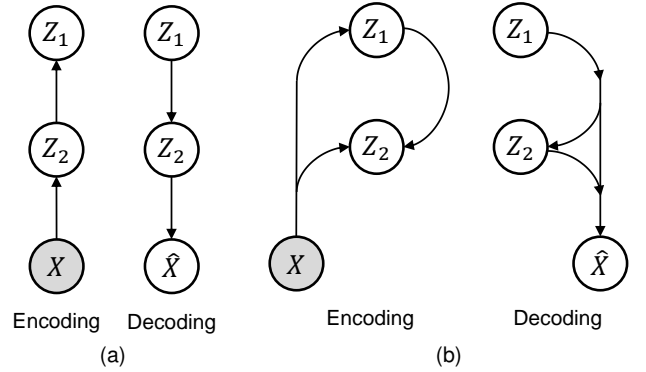


Fig. 2. Illustration of (a) a two-layer hyperprior VAE, and (b) a two-layer ResNet VAE. Detailed architecture of our ResNet VAE model is introduced in Sec. 3.

hierarchical ones [33], [34]. For lossy compression of continuous  $X$ , however, bits-back coding cannot be applied, and there lacks an entropy coding algorithm to code VAE latent variables into bits.

There are several lines of work that try to apply VAEs to lossy (image) compression. The first one is through relative entropy coding (REC) [8], where one wants to code samples of the latent variables with an average codelength close to the KL term in the VAE loss function (Eq. 3). Extensive research [8], [9], [35], [36] has been conducted towards this goal, but they either require an intractable execution time or incur a large codelength overhead. Another direction is to develop VAEs with discrete latent variables. Discrete VAEs (DVAEs) [37], [38], [39] assume Bernoulli latent variables, and Vector Quantized VAEs (VQ-VAEs) [40], [41], [42] assume categorical latent variables. Due to various statistical challenges, DVAEs and VQ-VAEs are still not capable of end-to-end R-D optimization in their current form.

Modern learned image coding methods mostly follow the Hyperprior structure [12], which can also be viewed as a type of hierarchical VAE. In the Hyperprior model, the latent variables are continuous during training but discretized during testing (*i.e.*, compression and decompression). Our work is largely inspired by it but is fundamentally different in the probabilistic structure, as we discussed in Sec. 2.3.

### 2.5 Variable-Rate Learned Image Compression

Various methods have been proposed to realize variable-rate compression using a single model. In an early work, Choi *et al.* introduce a conditional autoencoder with adjustable quantization bin size [43]. Chen and Ma propose to apply a post-training affine transform to modulate compressed coefficients [44]. Yang *et al.* propose a slimmable architecture with adjustable network complexity and compression rate [45]. Song *et al.* use a quality map to condition the compression model, enabling spatially-adaptive rate adjustment [46]. More recently, Cai *et al.* introduce an invertible neural network module that is conditioned on the quality level [47]. Lee *et al.* use a learnable mask to select the subset of compressed coefficients to compress [48]. Gao *et al.* directly optimize the compressed coefficients by semi-amortized inference for each specific R-D objective [49].

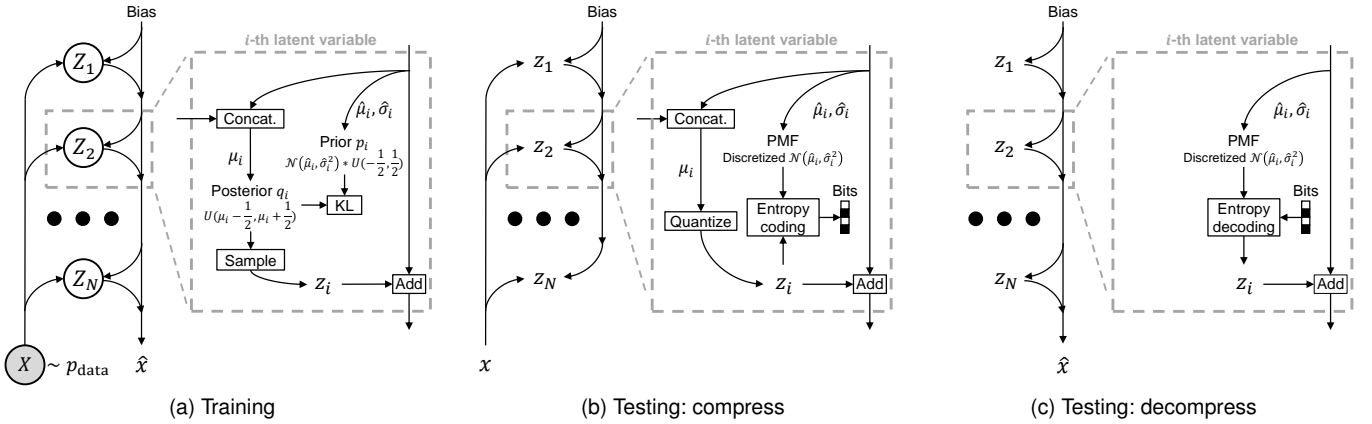


Fig. 3. Illustration of the quantization-aware ResNet VAE (QARV) model. Nodes with uppercase letters (e.g.,  $X, Z_1, Z_2, \dots$ ) denote *random* variables. Lower case letters (e.g.,  $\hat{x}, x, z_1, z_2, \dots$ ) denote *deterministic* variables or parameters.

Most existing methods either introduce non-trivial computational complexity or is difficult to be extended to hierarchical VAEs. In this paper, we introduce a new approach for variable rate compression (Sec. 4.4), which is simple, flexible, and yet effective.

### 3 QUANTIZATION-AWARE RESNET VAE (QARV)

In this section, we present the general framework of our QARV model, including its probabilistic model, training loss function, and how practical compression/decompression is done given a trained model. The framework is general and is independent of the neural network blocks used to implement it. In Sec. 4, we describe the specific neural network architecture that we use in our implementation.

#### 3.1 A Quantization-Aware Probabilistic Model

As we introduced in Sec. 1, we quantize the latent variables of ResNet VAEs so that existing entropy coding algorithms can be applied, and we redesign the probabilistic model of ResNet VAEs to support quantization-aware training. Our configuration resembles the mean & scale hyperprior entropy model [14] but extends it to a deep hierarchy of latent variables. We now give a formal description of our probabilistic model. For notational simplicity, we assume all variables (e.g., image  $x$  and latent variable  $z$ ) are scalars in our formulation. In the implementation, however, variables are multi-dimensional arrays, and we apply all the operations element-wise.

**Posteriors.** The posterior for the  $i$ -th latent variable  $Z_i$  is defined to be a (conditional) uniform distribution:

$$q_i \triangleq U\left(\mu_i - \frac{1}{2}, \mu_i + \frac{1}{2}\right) \Leftrightarrow q_i(z_i | z_{<i}, x) = \begin{cases} 1 & \text{for } |z_i - \mu_i| \leq \frac{1}{2} \\ 0 & \text{otherwise} \end{cases}, \quad (8)$$

where the parameter  $\mu_i$  is the output from the posterior branch in the  $i$ -th latent block (see Fig. 3a). The dependency of  $q_i(z_i | z_{<i}, x)$  on  $x$  and  $z_{<i}$  is made through  $\mu_i$ , which is a function of both  $x$  and  $z_{<i}$ . This leads to the bi-directional inference as we mentioned in Sec. 2.3.

Sampling from one posterior  $q_i$  can be easily implemented via additive uniform noise:

$$z_i \leftarrow \mu_i + u, \quad (9)$$

where  $u$  is a random sample from  $U(-\frac{1}{2}, \frac{1}{2})$ . To sample all latent variables  $z_1, z_2, \dots, z_N$ , one must sample them sequentially due to the autoregressive relationship between them. This additive noise can be viewed as a simulation of uniform quantization error, making the training process quantization-aware.

**Priors.** Given that the posteriors are uniform, the prior distribution must satisfy several requirements to enable efficient training and practical entropy coding. First, the prior probability density function (pdf) should be flexible enough to resemble a uniform distribution (since we minimize  $D_{\text{KL}}(q_i || p_i)$  in the VAE loss function). Second, the pdf must also be non-zero everywhere, otherwise evaluating  $D_{\text{KL}}(q_{Z|X} || p_Z)$  may result in a division by zero, causing numerical instabilities in training. Third, it should be easy to turn the prior pdf into a discrete probability mass function (pmf) to support practical entropy coding during testing.

A good choice that satisfies these requirements has been given in previous literature on learned image compression [12], [14]. We adopt a similar construction and extend it to the ResNet VAE architecture. Specifically, the prior distribution for  $Z_i$ , denoted by  $p_i$ , is chosen to be a (conditional) Gaussian convolved with a uniform distribution:

$$p_i \triangleq \mathcal{N}(\hat{\mu}_i, \hat{\sigma}_i^2) * U\left(-\frac{1}{2}, \frac{1}{2}\right) \Leftrightarrow p_i(z_i | z_{<i}) = \int_{z_i - \frac{1}{2}}^{z_i + \frac{1}{2}} \mathcal{N}(t; \hat{\mu}_i, \hat{\sigma}_i^2) dt, \quad (10)$$

where  $\mathcal{N}(t; \hat{\mu}_i, \hat{\sigma}_i^2)$  denotes the Gaussian pdf with mean  $\hat{\mu}_i$  and standard deviation  $\hat{\sigma}_i$  evaluated at  $t$ . The parameters  $\hat{\mu}_i$  and  $\hat{\sigma}_i$  are outputs of the prior branch in the  $i$ -th latent block (see Fig. 3a), and they are dependent only on  $z_{<i}$ , but not on the image  $x$ .

Sampling from the prior  $p_i(\cdot | z_{<i})$  can be done by using the reparameterization trick [28]:

$$z_i \leftarrow \hat{\mu}_i + \hat{\sigma}_i w + u, \quad (11)$$

where  $w$  and  $u$  are random samples from  $\mathcal{N}(0,1)$  and  $U(-0.5,0.5)$ , respectively.

**Training objective (fixed-rate).** The fixed-rate training objective is to minimize the ResNet VAE loss function (Eq. 7) with a pre-defined  $\lambda$ . Using our specified posteriors and priors, the loss function can be expressed as

$$\mathcal{L} = \mathbb{E}_{X, Z_{1:N}} \left[ \sum_{i=1}^N \log \frac{1}{p_i(Z_i | Z_{<i})} + \lambda \cdot d(X, \hat{X}) \right], \quad (12)$$

where the expectation is w.r.t.  $X \sim p_{\text{data}}$  and  $Z_{1:N} \sim q_{Z_{1:N}|X}$ , and recall that  $\hat{X}$  is a function of  $X$ . In practice, the expectation is estimated by drawing samples of  $X$  and  $Z_{1:N}$  from their respective distributions (also known as the Monte Carlo methods), and the neural network parameters are optimized using stochastic gradient descent (SGD) algorithms [50]. We can see that the first term in Eq. 12 corresponds to a continuous relaxation of the test-time bit rate (up to a constant factor), and the second term corresponds to the distortion. The multiplier  $\lambda$  trades off rate and distortion and is fixed throughout training. As a result, a separately trained model can compress images only at a fixed rate, which is inflexible in real-world applications and motivates the development of a variable-rate model.

**Training objective (variable-rate).** We adopt the conditional VAE [51] formulation for variable-rate compression. In this scheme, all priors and posteriors are conditional on  $\lambda$ , and continuous rate adjusting using a single model can be achieved simply by varying the  $\lambda$ . To train such a model, the loss function becomes

$$\mathcal{L} = \mathbb{E}_{X, \Lambda, Z_{1:N}} \left[ \sum_{i=1}^N \log \frac{1}{p_i(Z_i | Z_{<i}, \Lambda)} + \Lambda \cdot d(X, \hat{X}) \right], \quad (13)$$

where the expectation is w.r.t.  $X \sim p_{\text{data}}$ ,  $\Lambda \sim p_{\Lambda}$ , and  $Z_{1:N} \sim q_{Z_{1:N}|X, \Lambda}$ . In variable-rate training, the multiplier  $\Lambda$  becomes a random variable with a human-specified pdf  $p_{\Lambda}$ . We discuss our choice of  $p_{\Lambda}$  in Sec. 4.4. Similar to  $X$ , we sample a  $\lambda$  in each training iteration, and Eq. 13 is minimized using stochastic gradient descent. The dependence of the posteriors and priors on  $\lambda$  are made through their distribution parameters. This is done in practice by, *e.g.*, a hypernetwork [52] and sinusoidal embeddings [53].

## 3.2 Compression and Decompression

Once a QARV model is trained, it can be readily converted into a practical lossy compressor by quantizing and coding the latent variables in a way similar to the Hyperprior model [12]. We discuss the fixed-rate probabilistic model in this subsection, but the same process generalizes to our variable-rate model by simply conditioning all posteriors and priors on  $\lambda$ .

The procedure of compression is shown in Fig. 3b. Instead of sampling  $z_i$  from the posterior, we quantize the residual of  $\mu_i$  and  $\hat{\mu}_i$  to obtain  $z_i$ :

$$z_i \leftarrow \hat{\mu}_i + \lceil \mu_i - \hat{\mu}_i \rceil, \quad (14)$$

where  $\lceil \cdot \rceil$  denotes nearest integer rounding. In other words,  $\mu_i$  is quantized to its nearest neighbor from the set  $\{\hat{\mu}_i + n \mid$

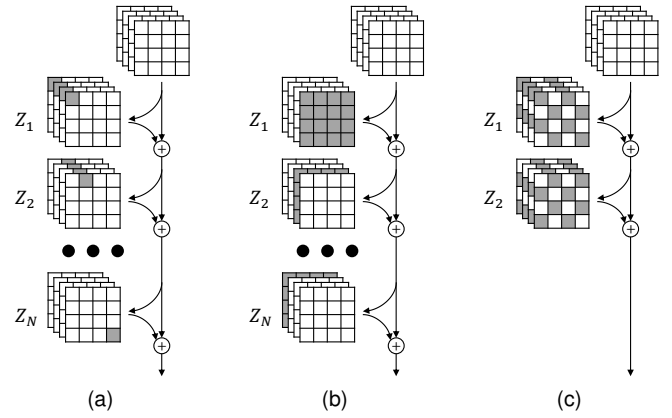


Fig. 4. Illustration of how QARV generalizes the AR context models in learned image compression methods, such as (a) the raster scan order AR model [14], (b) the channel-wise AR model [16], and (c) the Checkerboard model [15]. White blocks represent zeros, and gray blocks represent non-zero values.

$n \in \mathbb{Z}$ }. Then,  $z_i$  is encoded into bits using standard entropy coding algorithms, with pmf  $P_i$ :

$$P_i(n) \triangleq p_i(\hat{\mu}_i + n | z_{<i}), n \in \mathbb{Z}, \quad (15)$$

*i.e.*, the prior  $p_i$  evaluated at equally spaced values. Note that  $P_i(\cdot)$  is a valid pmf, or specifically, a discretized Gaussian [12]. Since each latent variable produces a separate bitstream, a compressed image consists of  $N$  bitstreams, corresponding to the  $N$  latent variables  $z_1, z_2, \dots, z_N$ .

The procedure of decompression is shown in Fig. 3c. Starting with a constant bias, we iteratively compute  $P_i$  for  $i = 1, 2, \dots, N$ . At each step, we apply the entropy decoding algorithm (with pmf  $P_i$ ) to decode  $z_i$  from the  $i$ -th bitstream. Note that  $P_i$  at the decoding side is the same as the one used in encoding, so exact  $z_i$  can be recovered. We can obtain the reconstruction  $\hat{x}$  once all latent variables  $z_{1:N}$  are decoded.

## 3.3 QARV Generalizes AR Context Models

A nice property of QARV (for both the fixed-rate and variable-rate versions) is that, if sufficiently deep, it generalizes autoregressive (AR) context models that are extensively used in existing learned image compression methods. Note that this conclusion holds for all types of autoregressive models, including the standard, raster scan order AR model [14], the channel-wise AR model [16], and the Checkerboard context model [15]. We illustrate this fact in Fig. 4, and we refer to [6] for the complete proof.

In principle, ResNet VAEs (and thus QARV) are able to learn better latent representations with possibly much fewer layers than autoregressive models [6]. Thus, by using QARV, one could avoid the manual process of designing the autoregressive order while outperforming autoregressive models, which we show in the experiments (Sec. 5.2).

## 4 NEURAL NETWORK IMPLEMENTATION

This section presents the neural network architecture we use to implement the (variable-rate) QARV model. We focus on variable-rate compression, as fixed-rate models are impractical in real-world applications. Our model architecture

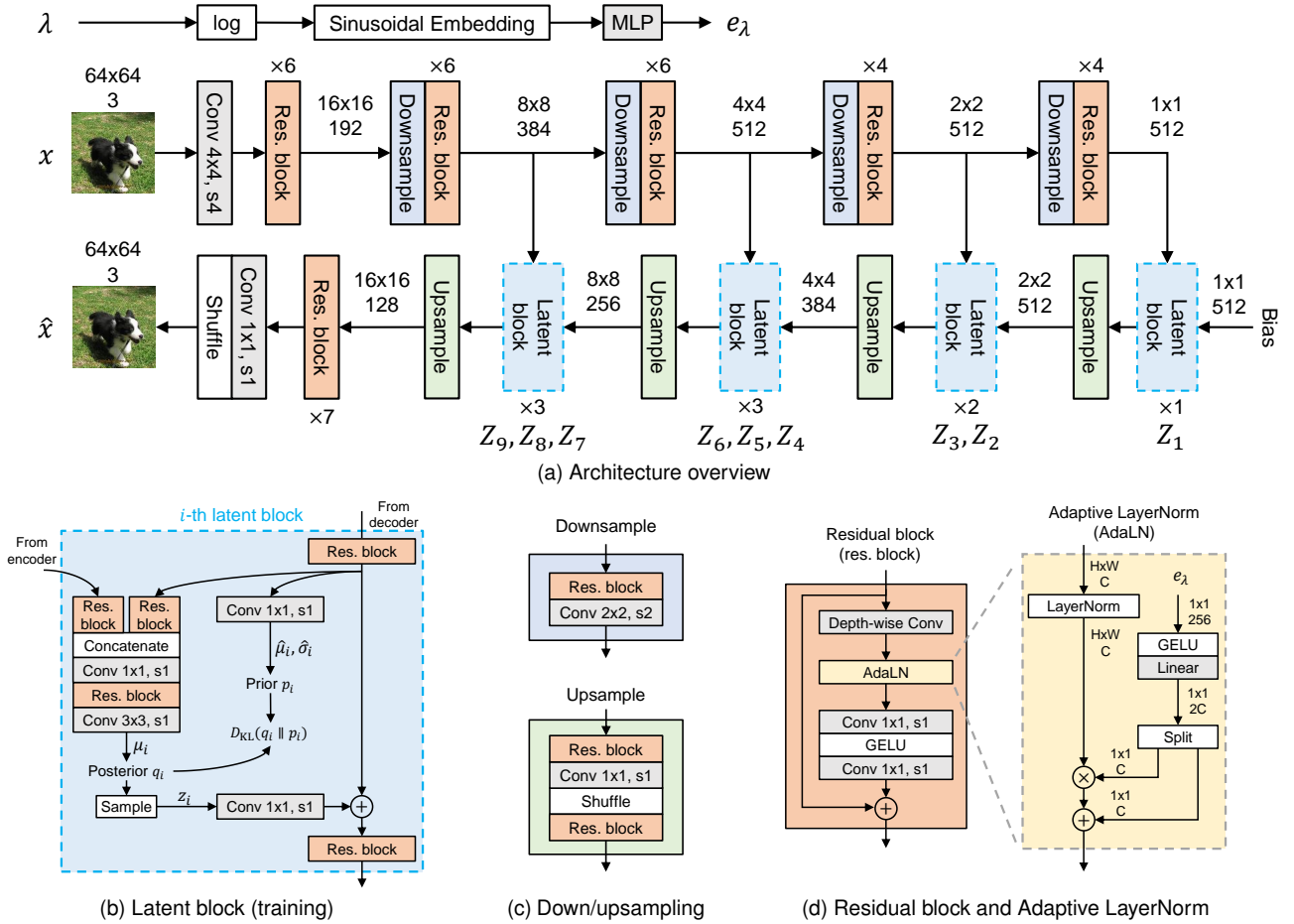


Fig. 5. **Neural network architecture of QARV.** White blocks denote non-parameterized operations. Colored (including gray) blocks denote parameterized neural network modules. Dimensions are for a  $64 \times 64 \times 3$  (height, width, and channel) image. Detailed explanations are provided in Sec. 4.

and its components are shown in Fig. 5. We describe each component in detail in the following subsections.

#### 4.1 Overall Architecture

Fig. 5a overviews the QARV model architecture. The model accepts two inputs, an image  $x$  to be compressed and a Lagrange multiplier  $\lambda$  that trade-offs rate and distortion. We overview the main model (lower part of Fig. 5a) in this subsection, and we introduce the  $\lambda$  embedding network (top part of Fig. 5a) in Sec. 4.4.

The main model architecture follows the QARV framework described in Sec. 3. On the encoding (sender) side, a CNN extracts a hierarchy of features (in total, 4 features) from the image, each having a different spatial resolution. We choose the feature resolutions to be 8x, 16x, 32x, and 64x downsampled w.r.t. the original input image resolution. For example, in Fig. 5a where the input image has  $64 \times 64$  pixels, the feature resolution ranges from  $8 \times 8$  to  $1 \times 1$ . These extracted features are then sent to the latent blocks in the decoding path (the right-to-left path) to produce the compressed bitstream. Each latent block corresponds to a latent variable from  $Z_1, Z_2, \dots, Z_9$  and produces a separate sequence of bits during encoding, and the collection of all such sequences forms the final bitstream to transmit.

On the decoding (receiver) side, only the right-to-left path in Fig. 5a is needed to decode the bitstream. The latent blocks and upsampling layers are executed in their sequential order, and a reconstruction image is obtained at the end of the path. This architecture naturally offers a bias towards faster decoding but slower encoding, since the entire network up to the last latent block corresponding to  $Z_9$  is executed during encoding, while only the decoding path is executed during decoding.

Our network architecture is fully convolutional, so when the input image resolution is multiples of  $64 \times 64$ , all feature resolution scales accordingly. For arbitrary resolution images, we simply pad the image (by replicating the edges) on the encoding side such that its resolution is multiples of  $64 \times 64$ . On the decoding side, we crop the reconstructed image to recover the original, un-padded image.

#### 4.2 A Latent Block Architecture for Fast Decoding

As we mentioned in Sec 1, decoding speed is more desired than encoding speed in practical applications, and ResNet VAEs naturally offer such bias toward fast decoding. To further promote this fact, we design a latent variable architecture, shown in Fig. 5b, that realizes efficient decoding. The left-hand side of the figure shows the posterior branch, and the middle part of the figure shows the prior branch.

Recall that both the posterior branch and the prior branch are needed for encoding  $z_i$ , but only the prior branch is needed for decoding  $z_i$ . The posterior branch consists of three residual blocks, a concatenation operation, and two convolutional layers, a combination of which fuses the features from the encoding path and the decoding path. In contrast to the posterior branch, the prior branch contains only a single convolutional layer, making decoding much more efficient than encoding.

### 4.3 Network Components

The downsampling and upsampling operators are shown in Fig. 5c. For downsampling, we use a convolutional layer whose stride equals the kernel size. This operator is also known as the patch embedding layer, which is commonly used in Vision Transformer architectures [54], [55]. Following [6], we put the patch embedding layer after a residual block to form a downsampling operator.

For upsampling, we use a  $1 \times 1$  convolution layer followed by pixel shuffling, which is also known as sub-pixel convolution [56]. One can view this as an inverse of the patch embedding layer. As shown in the bottom pane of Fig. 5c, the sub-pixel convolution is sandwiched between two residual blocks for additional non-linearity (since the sub-pixel convolution alone is purely linear).

The residual block architecture is shown in the left pane of Fig. 5d. Following our previous work [13], we adopt ConvNeXt [57] as our residual block architecture in favor of its efficiency. When the ConvNeXt block is used as is (as we did in [13]), the entire model is used for fixed-rate compression. To support variable-rate compression, we replace the Layer Normalization [58] in the original ConvNeXt block with the proposed adaptive Layer Normalization (AdaLN), which is described later in Sec. 4.4. The choice of the residual block is not restricted to ConvNeXt. Indeed, any block architecture that involves a Layer Normalization can be used with our method by replacing its Layer Normalization with AdaLN. In Sec. 5.3, we present experiments where we use our methods with the Swin Transformer block [55] and the Neighborhood Attention block [59].

### 4.4 Rate-Conditional Modules

Our model contains two modules that enable variable-rate compression: a  $\lambda$  embedding network (on top of Fig. 5a) and the AdaLN (right pane of Fig. 5d). We explain them one by one in this subsection.

**The  $\lambda$  embedding network** takes  $\lambda$ , a positive real number, as input and produces  $e_\lambda$ , a vector carrying information about  $\lambda$ . Given an input  $\lambda$ , we first scale it using a natural logarithmic function, motivated by the fact that most existing fix-rate compression methods choose  $\lambda$  evenly on a log scale. The scaled value is then converted into a vector using the sinusoidal embedding method, *i.e.*, the same method used for positional encoding in Transformers [53] and time embedding in diffusion probabilistic models [60]. Finally, a multilayer perceptron (MLP) is applied to improve non-linearity. The embedding  $e_\lambda$  is used in all residual blocks to make our model conditional on  $\lambda$ .

**Adaptive Layer Normalization (AdaLN):** the AdaLN module is built on the Layer Normalization [58] operation.

In the context of images, Layer Normalization normalizes (by subtracting the mean and dividing by the standard deviation) an image feature in the channel dimension, typically followed by an affine transform with learned weights and biases. In AdaLN (right pane of Fig. 5d), we parameterize the weights and biases of this affine transform as the output of a simple network whose input is  $e_\lambda$ . One can view this as using a hyper-network to produce the affine weights and biases of Layer Normalization. By doing this, the channel-wise mean and standard deviation of the output of AdaLN are determined by the output of the hyper-network, making residual blocks and thus the entire QARV model (including all posteriors and priors) conditional on  $\lambda$ .

**Training strategy.** Training is done by minimizing the variable-rate loss function (Eq. 13). Recall that one needs to manually specify  $p_\Lambda$ , *i.e.*, the distribution that  $\lambda$  is sampled from. The pdf  $p_\Lambda$  can be chosen arbitrarily to fulfill certain applications, for example, to assign more weights to a certain rate range. Given a lower bound  $\lambda_{\text{low}}$  and upper bound  $\lambda_{\text{high}}$ , we heuristically define  $p_\Lambda$  such that

$$\Lambda = \Delta^3 \text{ where } \Delta \sim U(\lambda_{\text{low}}^{-1/3}, \lambda_{\text{high}}^{-1/3}). \quad (16)$$

In other words,  $\Lambda$  is uniform in its cube root space. With this definition, the pdf  $p_\Lambda$  has a closed form expression:

$$p_\Lambda(\lambda) = \begin{cases} \frac{1}{\lambda_{\text{high}}^{-1/3} - \lambda_{\text{low}}^{-1/3}} \cdot \frac{1}{3} \lambda^{-2/3} & \text{if } \lambda_{\text{low}} \leq \lambda \leq \lambda_{\text{high}} \\ 0 & \text{otherwise.} \end{cases} \quad (17)$$

Our choice of  $p_\Lambda$  is motivated by the observation that uniform sampling in the cube root space of  $\lambda$  leads to a near-uniform sampling in the rate space. Note in particular that our QARV framework is not restricted to this specific choice of  $p_\Lambda$ .

## 5 EXPERIMENTS

### 5.1 Experiment Settings

**Datasets:** we use the COCO [63] dataset *train2017* split to train our model. It contains 118,287 images with around  $640 \times 420$  pixels. We randomly crop the images to  $256 \times 256$  patches during training. We evaluate our model on the following commonly-used test sets:

- **Kodak** [64]. This image set contains 24 images with either  $512 \times 768$  or  $768 \times 512$  pixels.
- **Tecnick TESTIMAGES** [65]. Following previous works [12], [14], we use the *RGB\_OR\_1200x1200* split, which contains 100 images with  $1,200 \times 1,200$  pixels. We refer to this test set as **Tecnick** for short.
- **CLIC 2022 test set**. This is the latest test set from the Challenge on Learned Image Compression (CLIC)<sup>1</sup>. It contains 30 images with around  $2048 \times 1365$  pixels. In this paper, we refer to this test set as **CLIC**.

**Metrics:** as standard practice, we report quality-rate curves instead of rate-distortion curves. We use peak signal-to-noise ratio (PSNR) to measure reconstruction quality:

$$\text{PSNR} \triangleq -10 \cdot \log_{10} \text{MSE}, \quad (18)$$

1. <http://compression.cc>

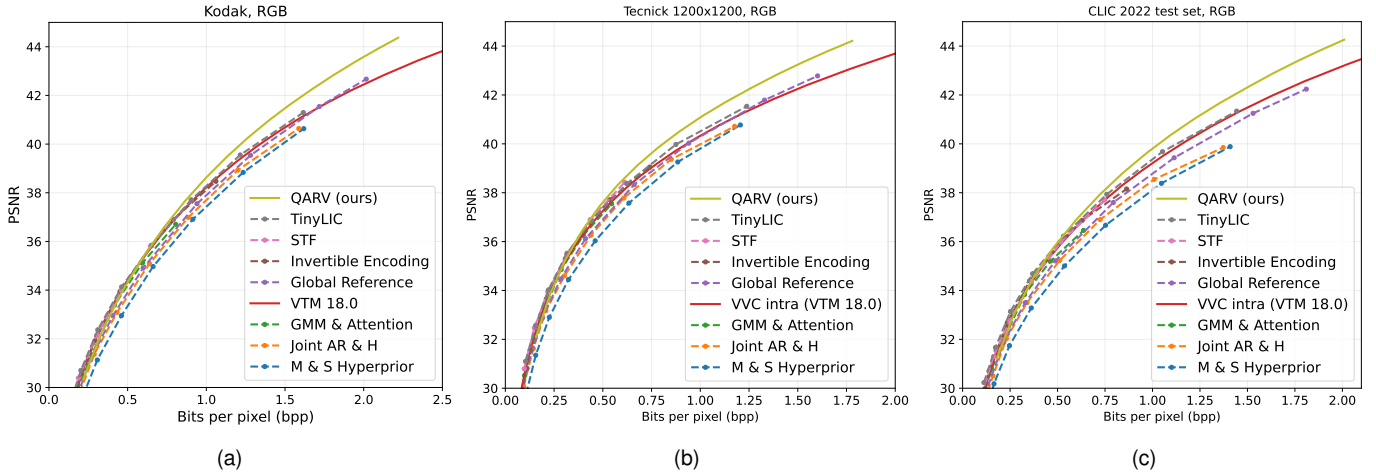


Fig. 6. **Lossy image compression efficiency on three test sets:** (a) Kodak, (b) Tecnick, and (c) CLIC 2022 test set. Dashed lines are fixed-rate methods (*i.e.*, separate models for different rates), and solid lines are variable-rate methods (*i.e.*, a single model with adjustable rates). Our QARV model, which supports variable-rate compression, achieves comparable PSNR with previous methods at low rates ( $\leq 0.5$  bpp) while outperforming them by a clear margin at high rates ( $> 0.75$  bpp).

TABLE 1  
Computational Complexity and BD-Rate of QARV Compared to Existing Learning-based Methods.

	# Models	# Params.	Latency (CPU)		Latency (GPU)		BD-rate (%) w.r.t. VTM 18.0			
			Enc.	Dec.	Enc.	Dec.	Kodak	Tecnick	CLIC	Avg.
<i>Variable-rate models</i>										
QARV (ours)	1	93.4M	0.880s	0.295s	0.211s	0.096s	-4.507	-8.431	-6.674	-6.537
<i>Parallel context models</i>										
TinyLIC [25]	8	227M	2.410s	2.489s	0.237s	0.316s	-3.100	-5.059	-5.573	-4.578
STF [24]	6	599M	0.644s	0.740s	0.139s	0.177s	-2.092	-6.219	-2.479	-3.597
M & S Hyperprior [14]	8	98.4M	0.194s	0.360s	0.053s	0.174s	21.99	22.06	27.56	23.87
<i>Non-parallel AR models</i>										
Invertible Encoding [61]	8	400M	2.324s	5.263s	2.170s	4.844s	0.338	-1.510	-2.154	-1.109
GMM & Attention [21]	6	115M	1.859s	4.921s	2.276s	4.978s	4.552	1.378	3.489	3.140
Global Reference [62]	9	324M	251.8s	259.6s	41.52s	49.76s	6.578	4.648	8.485	6.570
Joint AR & H [14]	8	158M	4.133s	7.322s	2.147s	5.169s	11.51	9.375	14.09	11.66

Testing environment: Intel 10700K CPU, Nvidia 1080 Ti GPU, Linux system, PyTorch 1.13, CUDA 11.7.

Latency is the average time to encode/decode a Kodak image ( $768 \times 512$  pixels), averaged over all 24 images. Time includes entropy coding.

where pixel values are between 0 and 1. PSNR is measured in the RGB space (not YUV). We measure data rate by bits per pixel (bpp):

$$\text{bpp} \triangleq \frac{\# \text{ of bits}}{\# \text{ of image pixels}}. \quad (19)$$

To obtain overall PSNR and bpp for an entire dataset, we first compute PSNR and bpp for each image and then average them over all images. We also use the BD-rate metric [66] to measure the average rate difference w.r.t. an anchor method (lower is better). We choose VVC intra codec [19] to be the BD-rate anchor in all our experiments.

**Training details:** For the main experiment in Sec. 5.2, we train our QARV model on COCO images for 2 million iterations with a batch size of 32. For other experiments including ablation studies, we train all models for 500k iterations with a batch size of 16. Other hyperparameters (*e.g.*, the optimizer and learning rate) stay the same across all experiments. We list the full training details in Appendix A.

## 5.2 Comparison with Existing Methods

We first compare QARV with existing open-source methods for lossy image compression. We use the recently developed VVC intra codec [19] (VTM version 18.0) as the BD-rate anchor. We list the details of all baseline methods, including the source of implementation and how we test them, in Appendix B.

The PSNR-bpp curves for the three test sets are shown in Fig. 6. Note in particular that most existing methods only support fixed-rate compression, while QARV is a variable-rate model. We observe that at lower rates ( $\leq 0.5$  bpp), most methods are comparable to each other, as the PSNR-bpp curves are highly overlapped. However, starting at around 0.75 bpp, our method outperforms other competitors by a clear margin, and the margin tends to grow larger as the rate increases. This observation is consistent across all three test sets as well as in our previous work [13]. We attribute this bias toward higher rates to the fact that QARV (9 stochastic layers) contains far more latent variables than

previous approaches (mostly 2 stochastic layers). More latent variables enable better coding of pixel details, making high-rate compression more efficient.

We report computational complexities and BD-rates of QARV against learning-based baseline methods in Table 1. The total number of parameters is summed over all separately trained models, and the encoding/decoding latencies are measured for the highest rate (to represent the worst-case scenario). In terms of the total number of parameters, QARV is more efficient than other methods, largely because it uses only a single model for all rates, while fixed-rate methods employ multiple models. In terms of CPU encoding latency, QARV is comparable with most existing methods within an order of magnitude. In terms of CPU decoding latency, however, QARV visibly outperforms all compared methods. Even when compared with the fastest baseline method, Mean & Scale Hyperprior [14], our approach still saves 18% of decoding time on CPU (0.295s vs. 0.360s). This feature of fast decoding may be favorable in many real-world applications where decoding speed is critical. The results for GPU encoding/decoding latency are similar to the ones for CPU. Our model is efficient in decoding latency, being the fastest one among all compared methods. In the last columns of Table 1, we report the BD-rate w.r.t. VTM version 18.0 (lower is better). We can observe that our approach achieves a better compression efficiency than all compared approaches. Overall, our QARV model is strong in both decoding latency and BD-rate, making it appealing in practice.

### 5.3 Additional Experiments

We conduct experiments to analyze the impact of different components of QARV, including network modules and training strategies, on compression efficiency.

**AdaLN vs. baseline methods.** We begin by comparing AdaLN with baseline variable-rate methods. The most relevant baseline method is the conditional autoencoder [43], where a conditional convolution (CConv) is proposed to replace standard convolutions. We implement CConv in our residual blocks, which is equivalent to placing the adaptive affine transform right after the depth-wise convolution (*i.e.*, position 1 in Fig. 7). In addition, we test other possible positions to place the affine transform in the ConvNeXt block, shown in Fig. 7. We train QARV for each possibility and report their performance in Table 2, where BD-rate is against VTM 18.0. We can observe that, among all positions, position 2 (*i.e.*, AdaLN) shows the best performance in terms of BD-rate, reflecting the effectiveness of the proposed method. Since the output of Layer Normalization has a zero mean and unit standard deviation (channelwise), the affine transform at position 2 directly determines the mean and std, which presumably leads to more efficient learning.

**Adaptive normalizations.** Instead of Layer Normalization, one could also use other types of normalization layers, such as Group Normalization [67] and Instance Normalization [68]. We experiment with Group/Instance Normalization by using them in place of Layer Normalization in QARV while keeping all other settings unchanged. Results are shown at the bottom of Table 2. Following [69], we use a group size of 32 for Group Normalization. In terms of

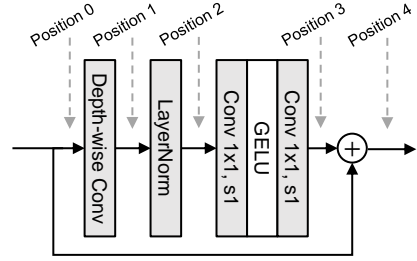


Fig. 7. Illustration of possible positions in a residual block to insert the adaptive affine transform for variable-rate compression. Inserting the affine transform at position 2 is equivalent to using AdaLN.

TABLE 2  
Comparison of Variable-Rate Compression Methods.

Affine Transform Position	Normalization	Kodak BD-rate (%)
Position 0	Layer Norm	2.446
Position 1 (CConv [43])	Layer Norm	2.005
Position 2 (AdaLN, ours)	Layer Norm	<u>0.576</u>
Position 3	Layer Norm	1.970
Position 4	Layer Norm	5.365
Position 2	Group Norm	1.041
Position 2	Instance Norm	10.26

BD-rate, we observe that Layer Normalization gives slightly better performance (by around 0.5% BD-rate) than Group Normalization, both of which significantly (by around 9.0% BD-rate) outperform the Instance normalization. We thus conclude that Layer Normalization (and thus our AdaLN) is a relatively better choice for lossy compression than other types of normalization.

**Choices of the Residual Block** We experiment with other types of residual blocks in addition to the ConvNeXt block. We adopt a recent Vision Transformer architecture, the Neighbourhood Attention Transformer (NAT) [59], to use in QARV. It also contains Layer Normalizations, and we replace the Layer Normalization in front of the MLP in each NAT block with AdaLN, in the same way as we did for ConvNeXt blocks. We show experimental results in Table 3, where for a fair comparison, we tune the number of channels of NAT blocks such that the total number of channels approximately match the ConvNeXt blocks. We observe that, with a comparable amount of parameters, the ConvNeXt block performs better than the NAT block by a margin of around 2% BD-rate. We thus use it as the choice of residual block in QARV.

**Range of  $\lambda$  during training.** We train QARV with different  $\lambda$  ranges and show R-D results in Fig. 9. We keep the lower bound  $\lambda_{\text{low}}$  fixed to 16, and vary the upper bound  $\lambda_{\text{high}}$  from 32 to 2048. As  $\lambda$  trades off rate and distortion, a wider range of  $\lambda$  results in a longer R-D curve. We first observe that, coarsely speaking, the R-D curves are mostly overlapped with each other. Interestingly, when looking at the lowest rate (corresponding to  $\lambda = 16$ ), the model with  $\lambda \in [16, 2048]$  gives the best R-D performance, indicating that training for high-rate compression also benefits low-rate compression. Overall, we can conclude that QARV generalizes to a wide range of rates.

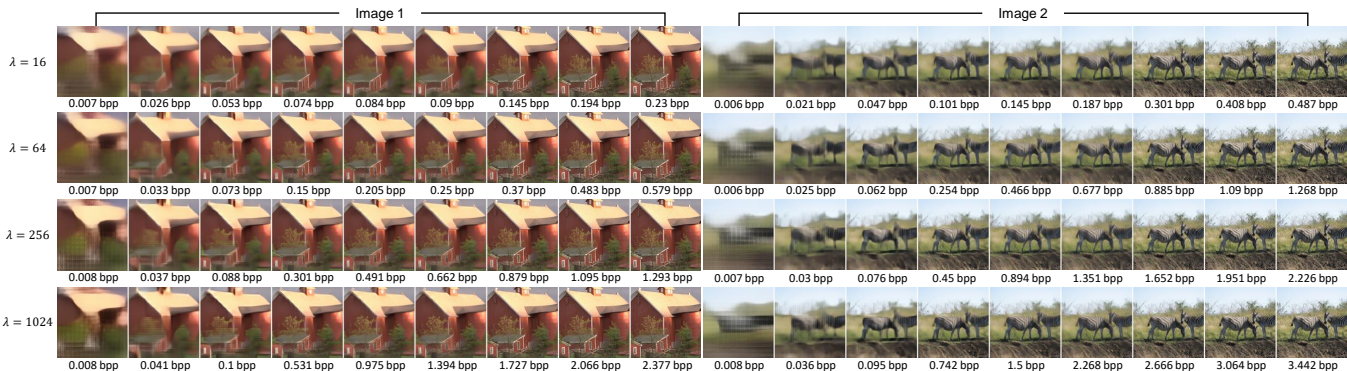


Fig. 8. **Examples of progressive coding results.** We decode only a subset of latent variables, and for the remaining latent variables, we use their prior mean instead. This could indicate what information is carried by each latent variable. Each row corresponds to a separate  $\lambda$  value. The images within each group (of 9 images), from left to right, correspond to the 9 latent variables  $Z_1, Z_2, \dots, Z_9$ . Image resolution is  $256 \times 256$ .

TABLE 3  
Comparison of the Choices of the Residual blocks.

Residual Block Type	# Params	Kodak BD-rate (%)
ConvNeXt [57]	93.4M	0.576
NAT [59]	103.6M	2.916

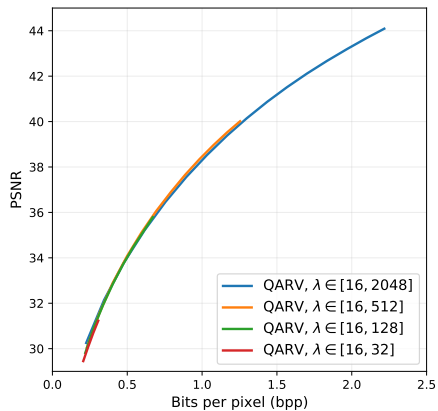


Fig. 9. Quality-rate curves on Kodak images of QARV trained with different  $\lambda$  ranges. We observe that a larger range of  $\lambda$  in training slightly improves PSNR at low rates.

## 5.4 Progressive Coding

A key feature of the QARV model is that it compresses (and decompresses) images starting from its low-dimensional features to its high-dimensional features, in a coarse-to-fine manner. We show examples for two images using various  $\lambda$  values in Fig. 8, where several interesting observations can be made. First, it is obvious that the first latent variable,  $Z_1$ , encodes “coarse features” of an image such as the brightness and color, shown in the leftmost image in each group. Note that  $Z_1$  consumes only a very small number of bits compared to the remaining latent variables, as it has the lowest dimension ( $64\times$  downsampled w.r.t. the original image). Second, the high-dimensional latent variables carry mostly imperceptible details in the image. For example, in the group of  $\lambda = 1024$  for image 1, the image with 1.394 bpp is almost visually indistinguishable from the image with 2.377 bpp. Lastly, the qualitative results suggest that the QARV model may be able to learn a semantic latent space. As can be seen in the second and third columns of results

for image 2, with no more than 0.1 bpp one could already recognize semantic information, such as the area of the sky, ground, and zebras.

The visual results for progressive decoding capture the hierarchical nature of images and could also be used for multi-task processing in the compressed domain (*e.g.*, using low-dimensional latent variables for classification while high-dimensional ones for segmentation). However, applying recent approaches for compressed domain object recognition [70], [71] to the hierarchical architecture is non-trivial, and we leave it to future work.

## 6 CONCLUSION

We have shown that deep ResNet VAEs can be used for practical lossy compression by applying test-time quantization and quantization-aware training. We present a novel lossy image compression framework, QARV, along with a neural network architecture for it. QARV provides a better compression efficiency than previous methods on three test sets, at the same time supporting variable-rate compression. The progressive coding scheme of QARV better matches human perception and leads to potential applications for compressed domain object recognition.

TABLE 4  
Training Hyperparameters.

	Main experiment	Ablation study
Training set	COCO 2017 train	COCO 2017 train
# images	118,287	118,287
Image size	Around 640x420	Around 640x420
Data augment.	Crop, h-flip	Crop, h-flip
Train input size	256x256	256x256
Optimizer	Adam	Adam
Learning rate	$2 \times 10^{-4}$	$2 \times 10^{-4}$
LR schedule	Constant + cosine	Constant
Weight decay	0.0	0.0
Batch size	32	16
# iterations	2M	500K
# images seen	64M	8M
Gradient clip	2.0	2.0
EMA	0.9999	0.9999
GPUs	$2 \times$ RTX 3090	$1 \times$ Quadro 6000
Time	260h	96h

TABLE 5  
Baseline Methods.

Method	Implementation
TinyLIC	<a href="https://github.com/lumingzzy/TinyLIC">https://github.com/lumingzzy/TinyLIC</a>
STF	<a href="https://github.com/Googolxx/STF/issues">https://github.com/Googolxx/STF/issues</a>
M & S Hyperprior	<a href="https://github.com/InterDigitalInc/CompressAI">github.com/InterDigitalInc/CompressAI</a>
Invertible Encoding	<a href="https://github.com/xyq7/InvCompress">github.com/xyq7/InvCompress</a>
GMM & Attention	<a href="https://github.com/InterDigitalInc/CompressAI">github.com/InterDigitalInc/CompressAI</a>
Global Reference	<a href="https://github.com/damo-cv/img-comp-reference">github.com/damo-cv/img-comp-reference</a>
Joint AR & H	<a href="https://github.com/InterDigitalInc/CompressAI">github.com/InterDigitalInc/CompressAI</a>

## APPENDIX A

### TRAINING DETAILS

We list detailed training information in Table 4, including data augmentation, hyperparameters, and devices. We use separate sets of training hyperparameters for the main experiment and the additional experiments, which are shown in the two columns, respectively.

## APPENDIX B

### BASILINE METHODS

**Learning-based image codecs.** In Table 1, we compare our QARV model with a number of learning-based image codecs in terms of computational complexity and BD-rate. We mentioned that we use open-source implementations of the baseline approaches for the experiments. We list the software implementations we used in Table 5. For a fair comparison, all methods are implemented using the PyTorch library.

## REFERENCES

- [1] S. Zhang, N. Kang, T. Ryder, and Z. Li, "iflow: Numerically invertible flows for efficient lossless compression via a uniform coder," *Advances in Neural Information Processing Systems*, pp. 5822–5833, Dec. 2021.
- [2] T. Ryder, C. Zhang, N. Kang, and S. Zhang, "Split hierarchical variational compression," *Proceedings of the IEEE/CVF Conference on Computer Vision and Pattern Recognition*, pp. 386–395, Jun. 2022.
- [3] T. M. Cover and J. A. Thomas, *Elements of Information Theory*. USA: John Wiley & Sons, Inc., 2006.
- [4] Y. Yang and S. Mandt, "Towards empirical sandwich bounds on the rate-distortion function," *International Conference on Learning Representations*, Apr. 2022.
- [5] D. P. Kingma, T. Salimans, R. Jozefowicz, X. Chen, I. Sutskever, and M. Welling, "Improved variational inference with inverse autoregressive flow," *Advances in Neural Information Processing Systems*, vol. 29, Dec. 2016.
- [6] R. Child, "Very deep vaes generalize autoregressive models and can outperform them on images," *International Conference on Learning Representations*, Apr. 2021.
- [7] J. Townsend, T. Bird, and D. Barber, "Practical lossless compression with latent variables using bits back coding," *International Conference on Learning Representations*, May 2019.
- [8] G. Flamich, M. Havasi, and J. M. Hernández-Lobato, "Compressing images by encoding their latent representations with relative entropy coding," *Advances in Neural Information Processing Systems*, vol. 33, pp. 16 131–16 141, Dec. 2020.
- [9] G. Flamich, S. Markou, and J. M. Hernández-Lobato, "Fast relative entropy coding with a\* coding," *Proceedings of the International Conference on Machine Learning*, vol. 162, pp. 6548–6577, Jul. 2022.
- [10] Y. Yang, R. Bamler, and S. Mandt, "Variational bayesian quantization," *Proceedings of the International Conference on Machine Learning*, vol. 119, pp. 10 670–10 680, Jul. 2020.
- [11] J. Ballé, V. Laparra, and E. P. Simoncelli, "End-to-end optimized image compression," *International Conference on Learning Representations*, Apr. 2017.
- [12] J. Ballé, D. Minnen, S. Singh, S. Hwang, and N. Johnston, "Variational image compression with a scale hyperprior," *International Conference on Learning Representations*, Apr. 2018.
- [13] Z. Duan, M. Lu, Z. Ma, and F. Zhu, "Lossy image compression with quantized hierarchical vaes," *Proceedings of the IEEE/CVF Winter Conference on Applications of Computer Vision*, pp. 198–207, Jan. 2023.
- [14] D. Minnen, J. Ballé, and G. Toderici, "Joint autoregressive and hierarchical priors for learned image compression," *Advances in Neural Information Processing Systems*, vol. 31, pp. 10 794–10 803, Dec. 2018.
- [15] D. He, Y. Zheng, B. Sun, Y. Wang, and H. Qin, "Checkerboard context model for efficient learned image compression," *Proceedings of the IEEE/CVF Conference on Computer Vision and Pattern Recognition*, pp. 14 766–14 775, Jun. 2021.
- [16] D. Minnen and S. Singh, "Channel-wise autoregressive entropy models for learned image compression," *Proceedings of the IEEE International Conference on Image Processing*, pp. 3339–3343, Oct. 2020.
- [17] G. Wallace, "The jpeg still picture compression standard," *IEEE Transactions on Consumer Electronics*, vol. 38, no. 1, pp. xviii–xxxiv, Feb. 1992.
- [18] A. Skodras, C. Christopoulos, and T. Ebrahimi, "The jpeg 2000 still image compression standard," *IEEE Signal Processing Magazine*, vol. 18, no. 5, pp. 36–58, Sep. 2001.
- [19] J. Pfaff, A. Filippov, S. Liu, X. Zhao, J. Chen, S. De-Luxán-Hernández, T. Wiegand, V. Rufitskiy, A. K. Ramasubramanian, and G. V. der Auwera, "Intra prediction and mode coding in vvc," *IEEE Transactions on Circuits and Systems for Video Technology*, vol. 31, no. 10, pp. 3834–3847, Oct. 2021.
- [20] J. Ballé, P. A. Chou, D. Minnen, S. Singh, N. Johnston, E. Agustsson, S. Hwang, and T. G. "Nonlinear transform coding," *IEEE Journal of Selected Topics in Signal Processing*, vol. 15, no. 2, pp. 339–353, Feb. 2021.
- [21] Z. Cheng, H. Sun, M. Takeuchi, and J. Katto, "Learned image compression with discretized gaussian mixture likelihoods and attention modules," *Proceedings of the IEEE/CVF Conference on Computer Vision and Pattern Recognition*, pp. 7936–7945, Jun. 2020.
- [22] T. Chen, H. Liu, Z. Ma, Q. Shen, X. Cao, and Y. Wang, "End-to-end learnt image compression via non-local attention optimization and improved context modeling," *IEEE Transactions on Image Processing*, vol. 30, pp. 3179–3191, Feb. 2021.
- [23] M. Lu, P. Guo, H. Shi, C. Cao, and Z. Ma, "Transformer-based image compression," *Data Compression Conference*, pp. 469–469, Mar. 2022.
- [24] R. Zou, C. Song, and Z. Zhang, "The devil is in the details: Window-based attention for image compression," *Proceedings of the IEEE/CVF Conference on Computer Vision and Pattern Recognition*, pp. 17 492–17 501, Jun. 2022.

- [25] M. Lu and Z. Ma, "High-efficiency lossy image coding through adaptive neighborhood information aggregation," *arXiv preprint arXiv:2204.11448*, Oct. 2022.
- [26] Y. Hu, W. Yang, Z. Ma, and J. Liu, "Learning end-to-end lossy image compression: A benchmark," *IEEE Transactions on Pattern Analysis and Machine Intelligence*, vol. 44, no. 8, pp. 4194–4211, Aug. 2022.
- [27] H. Ma, D. Liu, N. Yan, H. Li, and F. Wu, "End-to-end optimized versatile image compression with wavelet-like transform," *IEEE Transactions on Pattern Analysis and Machine Intelligence*, vol. 44, no. 3, pp. 1247–1263, Mar. 2022.
- [28] D. Kingma and M. Welling, "Auto-encoding variational bayes," *International Conference on Learning Representations*, Apr. 2014.
- [29] C. K. Sønderby, T. Raiko, L. Maaløe, S. r. K. Sønderby, and O. Winther, "Ladder variational autoencoders," *Advances in Neural Information Processing Systems*, vol. 29, Dec. 2016.
- [30] A. Vahdat and J. Kautz, "Nvae: A deep hierarchical variational autoencoder," *Advances in Neural Information Processing Systems*, vol. 33, pp. 19667–19679, Dec. 2020.
- [31] S. Sinha and A. B. Dieng, "Consistency regularization for variational auto-encoders," *Advances in Neural Information Processing Systems*, vol. 34, Dec. 2021.
- [32] G. E. Hinton and D. van Camp, "Keeping the neural networks simple by minimizing the description length of the weights," *Proceedings of the Sixth Annual Conference on Computational Learning Theory*, p. 5–13, 1993.
- [33] F. Kingma, P. Abbeel, and J. Ho, "Bit-swap: Recursive bits-back coding for lossless compression with hierarchical latent variables," *Proceedings of the International Conference on Machine Learning*, vol. 97, pp. 3408–3417, Jun. 2019.
- [34] J. Townsend, T. Bird, J. Kunze, and D. Barber, "Hilloc: lossless image compression with hierarchical latent variable models," *International Conference on Learning Representations*, Apr. 2020.
- [35] E. Agustsson and L. Theis, "Universally quantized neural compression," *Advances in Neural Information Processing Systems*, vol. 33, pp. 12367–12376, Dec. 2020.
- [36] L. Theis and N. Y. Ahmed, "Algorithms for the communication of samples," *Proceedings of the International Conference on Machine Learning*, vol. 162, pp. 21308–21328, Jun. 2022.
- [37] J. T. Rolfe, "Discrete variational autoencoders," *International Conference on Learning Representations*, Apr. 2016.
- [38] A. Vahdat, W. Macready, Z. Bian, A. Khoshman, and E. Andriyash, "Dvae++: Discrete variational autoencoders with overlapping transformations," *International Conference on Machine Learning*, pp. 5035–5044, Jul. 2018.
- [39] A. Vahdat, E. Andriyash, and W. Macready, "Dvae#: Discrete variational autoencoders with relaxed boltzmann priors," *Advances in Neural Information Processing Systems*, vol. 31, Dec. 2018.
- [40] A. van den Oord, O. Vinyals, and k. kavukcuoglu, "Neural discrete representation learning," *Advances in Neural Information Processing Systems*, vol. 30, Dec. 2017.
- [41] A. Razavi, A. van den Oord, and O. Vinyals, "Generating diverse high-fidelity images with vq-vae-2," *Advances in Neural Information Processing Systems*, vol. 32, Dec. 2019.
- [42] W. Williams, S. Ringer, T. Ash, D. MacLeod, J. Dougherty, and J. Hughes, "Hierarchical quantized autoencoders," *Advances in Neural Information Processing Systems*, vol. 33, pp. 4524–4535, Dec. 2020.
- [43] Y. Choi, M. El-Khamy, and J. Lee, "Variable rate deep image compression with a conditional autoencoder," *Proceedings of the IEEE/CVF International Conference on Computer Vision*, pp. 3146–3154, Oct. 2019.
- [44] T. Chen and Z. Ma, "Variable bitrate image compression with quality scaling factors," *IEEE International Conference on Acoustics, Speech and Signal Processing*, pp. 2163–2167, May 2020.
- [45] F. Yang, L. Herranz, Y. Cheng, and M. G. Mozerov, "Slimmable compressive autoencoders for practical neural image compression," *IEEE/CVF Conference on Computer Vision and Pattern Recognition*, pp. 4996–5005, Jun. 2021.
- [46] M. Song, J. Choi, and B. Han, "Variable-rate deep image compression through spatially-adaptive feature transform," *IEEE/CVF International Conference on Computer Vision*, pp. 2360–2369, Oct. 2021.
- [47] S. Cai, Z. Zhang, L. Chen, L. Yan, S. Zhong, and X. Zou, "High-fidelity variable-rate image compression via invertible activation transformation," *Proceedings of the ACM International Conference on Multimedia*, p. 2021–2031, Oct. 2022.
- [48] J. Lee, S. Jeong, and M. Kim, "Selective compression learning of latent representations for variable-rate image compression," *Advances in Neural Information Processing Systems*, Dec. 2022.
- [49] C. Gao, T. Xu, D. He, Y. Wang, and H. Qin, "Flexible neural image compression via code editing," *Advances in Neural Information Processing Systems*, Dec. 2022.
- [50] D. P. Kingma and J. Ba, "Adam: A method for stochastic optimization," *International Conference on Learning Representations*, May 2015.
- [51] K. Sohn, H. Lee, and X. Yan, "Learning structured output representation using deep conditional generative models," *Advances in Neural Information Processing Systems*, vol. 28, Dec. 2015.
- [52] D. Ha, A. M. Dai, and Q. V. Le, "Hypernetworks," *International Conference on Learning Representations*, Apr. 2017.
- [53] A. Vaswani, N. Shazeer, N. Parmar, J. Uszkoreit, L. Jones, A. N. Gomez, L. u. Kaiser, and I. Polosukhin, "Attention is all you need," *Advances in Neural Information Processing Systems*, vol. 30, Dec. 2017.
- [54] A. Dosovitskiy, L. Beyer, A. Kolesnikov, D. Weissenborn, X. Zhai, T. Unterthiner, M. Dehghani, M. Minderer, G. Heigold, S. Gelly, J. Uszkoreit, and N. Houlsby, "An image is worth 16x16 words: Transformers for image recognition at scale," *International Conference on Learning Representations*, May 2021.
- [55] Z. Liu, Y. Lin, Y. Cao, H. Hu, Y. Wei, Z. Zhang, S. Lin, and B. Guo, "Swin transformer: Hierarchical vision transformer using shifted windows," *IEEE/CVF International Conference on Computer Vision*, pp. 9992–10002, Oct. 2021.
- [56] W. Shi, J. Caballero, F. Huszár, J. Totz, A. Aitken, R. Bishop, D. Rueckert, and Z. Wang, "Real-time single image and video super-resolution using an efficient sub-pixel convolutional neural network," *Proceedings of the IEEE Conference on Computer Vision and Pattern Recognition*, pp. 1874–1883, Jun. 2016.
- [57] Z. Liu, H. Mao, C.-Y. Wu, C. Feichtenhofer, T. Darrell, and S. Xie, "A convnet for the 2020s," *Proceedings of the IEEE/CVF Conference on Computer Vision and Pattern Recognition*, pp. 11966–11976, Jun. 2022.
- [58] J. L. Ba, J. R. Kiros, and G. E. Hinton, "Layer normalization," *arXiv preprint arXiv:1607.06450*, Jul. 2016.
- [59] A. Hassani, S. Walton, J. Li, S. Li, and H. Shi, "Neighborhood attention transformer," *arXiv preprint arXiv:2204.07143*, Nov. 2022.
- [60] J. Ho, A. Jain, and P. Abbeel, "Denoising diffusion probabilistic models," *Advances in Neural Information Processing Systems*, vol. 33, pp. 6840–6851, Dec. 2020.
- [61] Y. Xie, K. L. Cheng, and Q. Chen, "Enhanced invertible encoding for learned image compression," *Proceedings of the ACM International Conference on Multimedia*, p. 162–170, Oct. 2021.
- [62] Y. Qian, Z. Tan, X. Sun, M. Lin, D. Li, Z. Sun, L. Hao, and R. Jin, "Learning accurate entropy model with global reference for image compression," *International Conference on Learning Representations*, May 2021.
- [63] T. Lin, M. Maire, S. Belongie, J. Hays, P. Perona, D. Ramanan, P. Dollár, and C. L. Zitnick, "Microsoft coco: Common objects in context," *Proceedings of the European Conference on Computer Vision*, pp. 740–755, Sep. 2014.
- [64] E. Kodak, "Kodak lossless true color image suite," <http://r0k.us/graphics/kodak/>.
- [65] N. Asuni and A. Giachetti, "TESTIMAGES: a Large-scale Archive for Testing Visual Devices and Basic Image Processing Algorithms," *Smart Tools and Apps for Graphics - Eurographics Italian Chapter Conference*, Sep. 2014.
- [66] G. Bjontegaard, "Calculation of average psnr differences between rd-curves," *Video Coding Experts Group - M33*, Apr. 2001.
- [67] Y. Wu and K. He, "Group normalization," *Proceedings of the European Conference on Computer Vision*, Sep. 2018.
- [68] X. Huang and S. Belongie, "Arbitrary style transfer in real-time with adaptive instance normalization," *Proceedings of the IEEE International Conference on Computer Vision*, pp. 1510–1519, Oct. 2017.
- [69] P. Dhariwal and A. Nichol, "Diffusion models beat gans on image synthesis," *Advances in Neural Information Processing Systems*, vol. 34, pp. 8780–8794, Dec. 2021.
- [70] K. Xu, M. Qin, F. Sun, Y. Wang, Y. Chen, and F. Ren, "Learning in the frequency domain," *Proceedings of the IEEE/CVF Conference on Computer Vision and Pattern Recognition*, pp. 1737–1746, Jun. 2020.
- [71] Z. Wang, M. Qin, and Y.-K. Chen, "Learning from the cnn-based compressed domain," *Proceedings of the IEEE/CVF Winter Conference on Applications of Computer Vision*, pp. 4000–4008, 2022.